Journal of Power Sources 315 (2016) 236–241

Contents lists available at ScienceDirect

Journal of Power Sources

journal homepage: www.elsevier.com/locate/jpowsour

Polyvinyl alcohol gelation: A structural locking-up agent and carbon source for Si/CNT/C composites as high energy lithium ion battery anode

Dingqiong Chen, Wenjuan Liao, Yang Yang, Jinbao Zhao*

College of Chemistry and Chemical Engineering, State Key Laboratory of Physical Chemistry of Solid Surfaces, Collaborative Innovative Center of Chemistry for Energy Materials, Xiamen University, Xiamen 361005, China

HIGHLIGHTS

- A facile method is developed to fabricate Si/CNT/C composites.
- PVA hydrogel is acted as both locking-up agent and carbon source in composites.
- The Si/CNT/C composites exhibit excellent capacity retention.

GRAPHICAL ABSTRACT

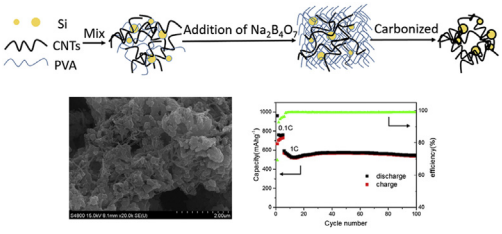

ARTICLE INFO

Article history:
Received 30 January 2016
Received in revised form
10 March 2016
Accepted 13 March 2016
Available online 21 March 2016

Keywords:
Polyvinyl alcohol hydrogel
Locked up
Silicon
Lithium-ion battery

ABSTRACT

A novel polyvinyl alcohol (PVA) hydrogel method is developed to synthesize Si/CNT/C composites. The Si nanoparticles and CNTs are 'position' locked up by PVA hydrogel in a simple aqueous solution process, and then the Si-CNT-PVA hydrogel has pyrolyzed to form Si/CNT/C composites. In this unique structured Si/CNT/C composites, the CNTs form a porous network acting both as conductive agent for electron transfer and buffer space to accommodate huge Si volume change during lithiation/delithiation process, while the coating layer of carbon carbonized from polyvinyl alcohol (PVA) hydrogel is conducive to stabilize the interweaved composite structure. The complex structures of Si/CNT/C composites and their electrochemical properties are presented in this paper. The Si/CNT/C composites exhibit an initial reversible capacity of nearly 800 mAhg^{-1}, an excellent capacity retention of 97.1% after 100 cycles at the rate of 0.1 C, and high capacity retention even at high current rate.

1. Introduction

Owing to their high energy density and excellent cycle stability, lithium ion batteries (LIBs) are widely used in consumer electronics and electric vehicles [1–3]. Graphite is the commercially dominant anode material for LIBs at present, but its limited theoretic capacity (372 mAhg^{-1}) cannot fully satisfy the requirement of the high energy density in vehicle battery. Hence research efforts have been devoted significantly to the developing of high capacity anode materials for LIBs [1,4]. Among the materials studied, silicon is a promising candidate to replace graphite as the anode in LIBs due to its highest theoretical specific capacity (4200 mAhg^{-1}) [5–7]. However, due its low intrinsic electric conductivity and dramatic volume change (~300%) in the process of lithiation and delithiation [8–11], which results in electrode pulverization and capacity loss with cycling [5,12–14], the application of silicon as anode in LIBs was severely hindered. It was discovered that the pulverization

* Corresponding author.
E-mail address: jbzhao@xmu.edu.cn (J. Zhao).

http://dx.doi.org/10.1016/j.jpowsour.2016.03.051
0378-7753/

effect of silicon during lithiation/delithiation is strongly size dependent [15,16]. Silicon particles smaller than 150 nm in diameter or silicon nanowires smaller than 300 nm in diameter can survive the volume expansion/shrinkage and retain their structures even though the SEI (solid electrolyte interphase) on silicon surface is under constant rupture and reformation. Thus intense studies were focused on enhancing the capacity retention by creating exotic silicon nanostrcutures [17–20]. However, these complicated silicon nanostructures are only available in tiny quantity and extremely expensive and cumbersome for mass production, thus inapplicable for LIBs.

Another effective approach is to confine Si particles inside a conductive matrix to create a composite structure [21–25]. The conductive matrix could not only improve the electrical conductivity of the whole electrode, but also prevent the aggregation of Si particles and accommodate the large Si volume change during discharge/charge process [21,24–28]. Synthesis of Si/C composites is an effective and inexpensive solution because of the intrinsic high electrical conductivity of carbon. Carbon coasting is also advantageous for LIBs because the SEI formed on carbon surface is much more stable than that formed on silicon surface. Many synthetic processes for Si/C composites, such as mechanically milled [26,29], spray drying [25], electrospinning [30] or complex chemical reactions [21,28,31], have been developed and the composite materials produced were proved to enhance their electrochemical performance compared to bare silicon, but no satisfactory result was yet achieved. Herein, we report a simple and efficient method through polymerization reaction to fabricate silicon hybrid composites from interweaved networks of CNTs and PVA hydrogel, which were pyrolyzed to form Si/CNT/C composites as high energy anode materials. PVA itself has been commonly used as carbon source for silicon surface coating [26,32–34], but PVA hydrogel technology was not employed in material processing for LIBs, although it is widely applied in many different areas of biotechnology [35,36]. Compared to pyrolysis of PVA (or other organics), a commonly used method for carbon coating on silicon particles in which PVA is in fluid state when melt before pyrolysis and all solids are “floating” and thus it is prone to phase segregation during pyrolysis, PVA hydrogel can lock up Si particles and CNTs in a rigid hydrogel structure which leads to better contact between Si particles and CNTs after pyrolysis of PVA hydrogel. In this paper, we will demonstrate the feasibility of the PVA hydrogel applied to the synthesis of hybrid Si/CNT/PVA and Si/CNT/C composites. The electrochemical properties of the Si/CNT/C composites will also be presented.

2. Experiment

2.1. Synthesis

0.3 g Si nano-particles (ca 100 nm, Huierna, Henan) and 0.075 g MWCNT (OD > 50 nm, length 10–20 μm, purity >95%, Chengdu Organic Chemical Co., Ltd, China) were added to a 5 wt% aqueous polyvinyl alcohol (PVA-124, Dahao Chemical Co., Shantou) solution. The mixture was sonicated and then stirred for 12 h at room temperature. A hydrogel formed immediately after 12 ml sodium borate (purity >99.5%, AR, Xilong Chemical Co.) solution (with 0.6 g solute) added to above mixture. The weight ratio of Si, CNTs, PVA and Sodium borate was fixed to 4:1:8:8. The sample was named S4 (Si/CNT/C). In order to investigate the effect of CNTs and sodium borate, we also carried out comparative experiments: S1 (Si/C), Si mixed with PVA and then the solution frozen by liquid nitrogen; S2 (Si/C), Si mixed with PVA and then formed hydrogel with the addition of sodium borate; S3 (Si/CNT/C), Si mixed with PVA and CNTs frozen by liquid nitrogen. The obtained samples were freeze-dried, and then heated to 800 °C at a speed of 5 °C for 4 h in argon atmosphere. For comparison, the synthesis parameters of the four samples were summarized as follows (Table 1).

2.2. Characterization

The crystal structures of the as-obtained samples were characterized by X-ray diffraction (Rigaku MiniFlex 600) using Cu Kα radiation. The microstructures of the composites were characterized by field emission scanning electronic microscope (FE-SEM, S-4800, Hitachi), and X-ray energy spectroscopy (EDS, OXFORD 7593-H) was used to analyze the element content of the samples with 15 kV acceleration voltage. The DSC/TG (STA 449 F3 Jupiter Netzsch) was carried out to measure the silicon content of materials.

2.3. Electrochemical test

The electrode mixture was composed of synthesized active materials, acetylene black and poly (acrylic acid)/sodium carboxymethyl cellulose (wt/wt = 1/1) binder with a ratio of 6:3:1 (in weight). The aqueous slurry of the electrode mixture was spread onto a copper foil and dried at 80 °C for 10 h under vacuum. The electrochemical performance of materials were evaluated by 2016-type coin cells, which lithium foil were used as both the counter and reference electrodes. Celgard 2400 membrane was used as the separator and the electrolyte is a solution of 1 M $LiPF_6$ in EC/DMC/DEC (1/1/1 V/V/V) with 5 wt% fluorinated ethylene carbonate as additive. The coin cells were cycled at various current rates (0.1–5 C) between 0.02 V and 1.5 V vs Li^+/Li using a LAND-CT2001A battery test system (LAND Electronic Co., China). The Cyclic Voltammetry (CV) was measured on a CHI660D electrochemical workstation at a scanning rate of 0.01 mV^{-1} with voltage ranging from 0.02 to 2.3 V. The electrochemical impedance spectra (EIS) of all the samples were tested in the frequency range of 10 mHz–100 kHz via Solartron 1287-1260 Electrochemical workstation. All these electrochemical tests were tested at room temperature.

3. Results and discussion

The general scheme of the polymerization-carbonized process to fabricate Si/CNT/C composites was illustrated in Fig. 1a. The Si nanoparticles and CNTs were added to PVA solution under stirring. The mixture was sonicated and then stirred for 12 h at room temperature, so as to be evenly mixed to obtain a homogenous aqueous solution (Fig. 1b). When the gelation agent (sodium borate) was added, the hydrogel formed immediately (Fig. 1c). The final step was to pyrolyze the hybrid gel at an elevated temperature to form Si/CNT/C composites (S4).

The morphologies of the Si/C and Si/CNT/C composites prepared were presented in Fig. 2. Compared Fig. 2a,b, it can be seen that the morphology of composites from PVA hydrogel coating is quite different from that of mere PVA coating. The PVA hydrogel coated composites show a continuous homogeneous coating layer (Fig. 2b); the mere PVA coated composites (Fig. 2a), on the other hand, looks like a stack of articles, thus it is obvious that PVA hydrogel coating is beneficial to prevent the aggregation of Si particles (compare with Si nanoparticles raw materials in Fig. S2a in the Supporting Information). The adding of CNTs does not change the morphology of sample of mere PVA coating as shown in Fig. 2c except the observation of CNTs. However, the adding of CNTs does change the morphology of sample from PVA hydrogel coating to some extent. The carbon coating layer is not as smooth as that without CNTs, the continuous network of carbon coating is breaking down and the particle size is also smaller (Fig. 2d). The

Table 1
Samples composition and preparation condition.

Sample	S1	S2	S3	S4
silicon	+	+	+	+
PVA	+	+	+	+
CNTs	−	−	+	+
Sodium borate	−	+	−	+
Reaction manner	Freezing by liquid nitrogen	crosslinking	Freezing by liquid nitrogen	crosslinking

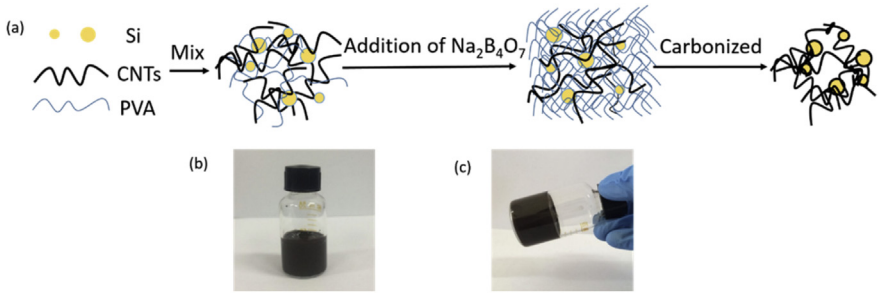

Fig. 1. (a) Schematic of the polymerization-carbonized process to fabricate S4 (Si/CNT/C composites) using Si nanoparticles, CNTs and PVA; (b) Photograph of the solution consists of Si nanoparticles, CNTs and PVA; (c) Photograph of hybrid PVA hydrogel mixed with Si nanoparticles and CNTs.

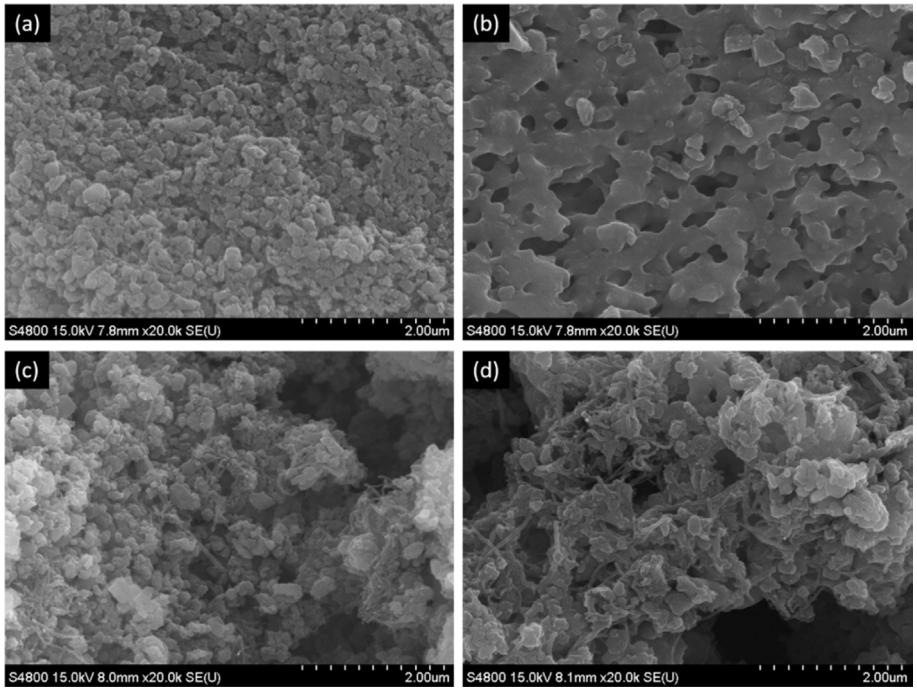

Fig. 2. SEM images of the sample S1 (a), S2 (b), S3 (c) and S4 (d).

CNTs network is slightly more uniform than that in mere PVA coating which indicates a structure "lock-up" ability of PVA hydrogel to stabilize the Si/CNTs composites. The silicon content was determined to be 26.19% in the S4 from the TGA profile shown in Fig. S3. While EDS analysis shows that the silicon content is 32.13% in the S4 (Table S1), which is comparable to the result of TGA.

Fig. 3 shows the XRD patterns of all the samples. From Fig. 3a-d, it is seen that all the samples show well-defined peaks at 2θ of 28.4, 47.4, 56.2,69.2, 76.5, and 88.1°, which can be indexed to the (111), (220), (311), (400), (331), and (422) planes of crystallized Si (JCPDS No. 00-026-1481) [37]. Thus, our hydrogel coating process does not alter the Si nanoparticles crystal structure. No carbon peak was found in the XRD pattern, indicating that the coated carbon is amorphous, agreed well with previous reports [21,29]. The few new peaks showed up in Fig. 3b and d were due to the addition of sodium borate.

The cycling performance of all samples is shown in Fig. 4a. All capacities were calculated on the basis of the total weight of composite materials including the coated carbon, CNTs, and Si. The initial capacity of S1 is low and its capacity increases gradually as the cycling continues. The Si/C composites from PVA hydrogel is even worse as the initial capacity is lower and the activation cycling is much longer, which is probably due to the "perfect" carbon

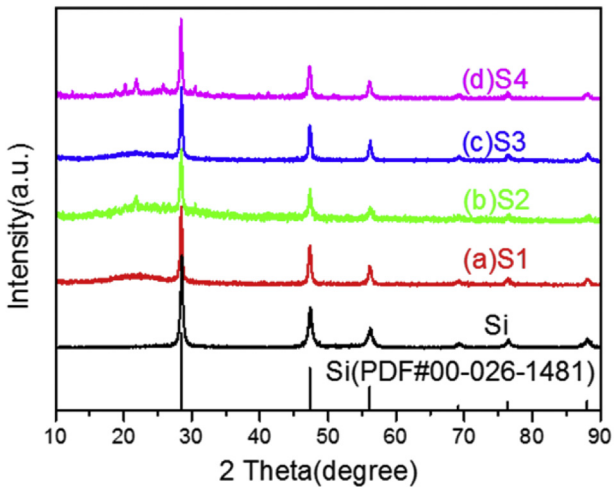

Fig. 3. X-ray diffraction patterns of sample S1 (a), S2 (b), S3 (c) and S4 (d).

and charge capacities of 1331 mAhg^{-1} and 817 mAhg^{-1}, respectively. While the capacity of S3 fades with the capacity retention of only 67.9% after 100 cycles, similar decay rate to that of S1. The S4 electrode exhibits slightly lower initial charge/discharge capacities (795 mAhg^{-1} and 1168 mAhg^{-1}, respectively) due to the added weight of sodium borate, but a similar coulombic efficiency of 68.1%. However, it demonstrates a much improved cyclability with the charge capacity retention of 97.1% after 100 cycles at the rate of 0.1 C. The high rate performance of S4 sample is shown in Fig. 4b. The capacity retention at the rate of 1 C of S4 is 71.7% to its 0.1 C capacity and 91.9% if compared to its first 1 C discharge capacity (the 6th cycle). The rate capability of S4 electrode is shown in Fig. 4c. It performs well at high current density. For example, at a current rate of 5 C, S4 still delivers a charge capacity of 390 mAhg^{-1}. When the current rate was returned to 0.1C, the charge capacity is 773 mAhg^{-1}, which is 96% of the initial reversible capacity.

The cyclic voltammetry (CV) of S4 is shown in Fig. 4d. It shows the first five cycles of the S4 between 0.02 V and 2.3 V at a potential sweep rate of 0.01 mVs^{-1}. The small peak at around 1.2 V in the first

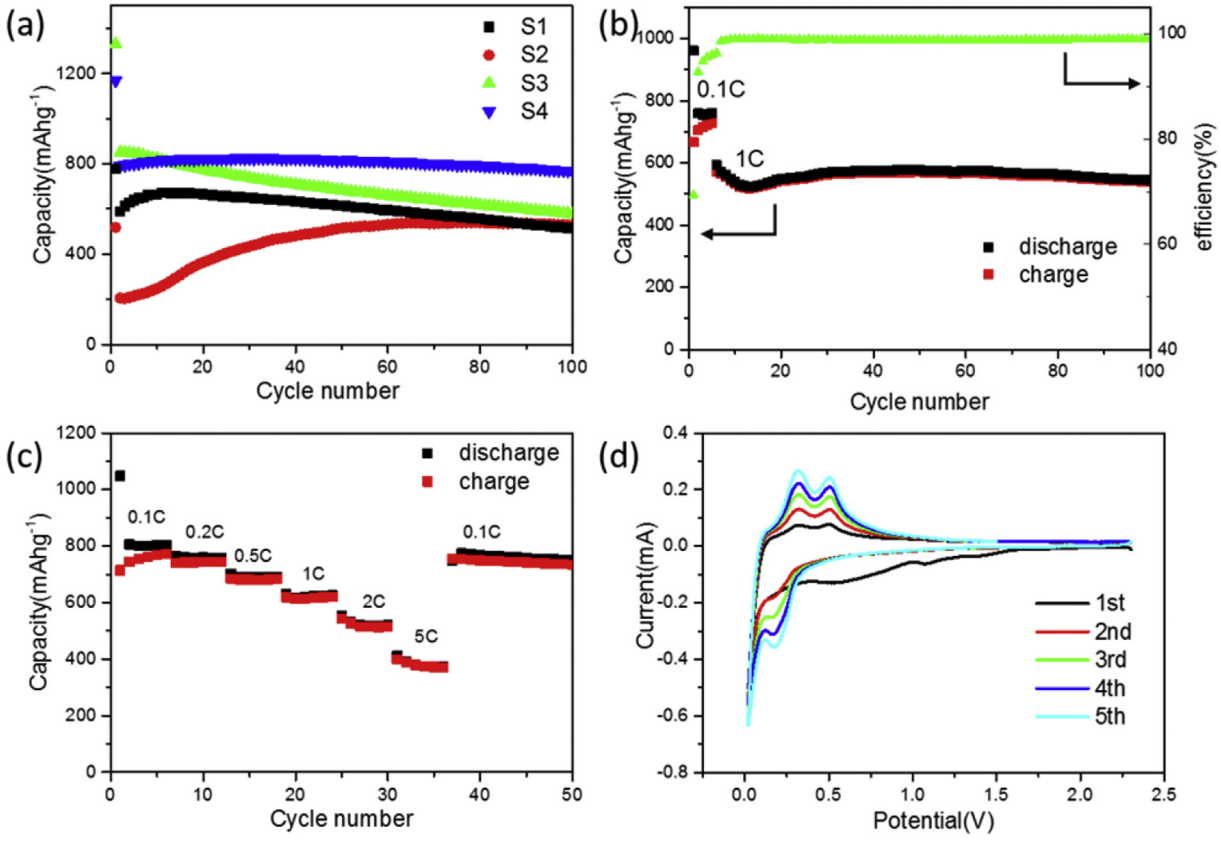

Fig. 4. (a) Cycling performance of all products at the rate of 0.1C; (b) Cycling performance of S4 at the rate of 1C; (c) Cycling performance of S4 at various current densities; (d) Cyclic voltammetry profiles of S4.

coating from PVA hydrogel as shown in Fig. 2b which results in a very slow ion conducting through the carbon layer, however, after its charge capacity reaches stable stage, it does not decay compared to the S1 electrode. The introduction of CNTs into the composites facilitates electric conductivity, and the initial capacities of the composites S3 and S4 are higher compared to S1 and S2. Also the activation process is only a few cycles, which indicates that the porous CNTs framework is in favor of electrolyte infiltration. The initial coulombic efficiency of S3 is 61.4%, with an initial discharge cycle can be attributed to the decomposition of the FEC additive in the electrolyte [38], the broad peak at around 0.56 V only appeared in the first cycle, not in subsequent cycles, and no obvious oxidation peak corresponding to this reduction process is observed in the anodic branch, suggesting that it is due to the formation of solid electrolyte interphase (SEI) on the electrode surface. The reaction of crystalline silicon with lithium to form amorphous Li_xSi appears below 0.1 V [39]. In the cathodic sweep of the following CV curve, there are two peaks at around 0.051 and 0.17 V, associated with the

formation of different phases of Li–Si alloy ($Li_{12}Si_7$ and $Li_{12}Si_4$) [40]. Correspondingly, the two anodic peaks at 0.32 and 0.51 V can be corresponding to the de-alloying of Li–Si alloys [41]. The gradually increase of both cathodic and anodic peaks current can be ascribed to the activation of more active Si in composites, which has been reported in previous studies [42,43]. Our results are well consistent with many previously reported in the literature [38–43].

To further understand the reason for the improved cyclability of the sample electrodes, the electrochemical impedance spectroscopy (EIS) measurements were performed on the cells after five cycles. Fig. 5 shows the Nyquist plots of the four electrodes with the equivalent circuit as inset. All of the samples display two well-defined semicircles. The former semicircle in high frequency region is generally connected to Li ion migration through surface layers, while the latter one to the Li ion transfer through interfaces. In addition, an inclined line in the low-frequency range is considered as Warburg impedance [44]. Even though the amplitude of the second semicircle of each sample varies, but the variation is much smaller than that of the first circle, thus the charge transfer resistance (R_{ct}) dominates the total impedance of the electrode. The R_{ct} is calculated to be 67.27, 148.6, 62.22 and 13.91 Ω cm^{-2} for each of the four sample electrode. The S4 electrode exhibits the smallest R_{ct} among the four sample electrodes, indicating the enhanced ionic conductivity of S4.

Among the four samples studied, S4 exhibits the best charge capacity retention with only few activation cycles. The superior of S4 can be attributed both to the presence of CNTs and the PVA hydrogel coating. The PVA hydrogel coating can “lock up” the silicon particles to prevent their aggregation and also “lock up” the relative positioning of Si particle and CNTs to prevent them from separation to ensure a good contact. The CNTs form a network for good electric conductivity. It also brings an unexpected effect, i.e., preventing formation of big agglomerate of silicon particles. The porous network facilitates electrolyte infiltration and lithium ion conductivity, and provides a buffer space for accommodating the huge volume change during silicon lithiation/delithiation process. As a result of these corporative effects, the Si/CNT/C composites material shows high charge/discharge capacities, high capacity retention and good rate capability.

4. Conclusions

In summary, we have successfully developed a simple and efficient method through polymerization reaction to fabricate high performance Si/CNT/C composites using PVA hydrogel as carbon source. In the unique structure, Si nanoparticles are well-dispersed in porous CNTs networks with buffer space to accommodate the severe volume change and enhance electric/ionic conductivities, while the PVA hydrogel and carbon coating layer formed after pyrolysis locks up the stable electric conductive network for active Si, eventually leads to better cycling performance.

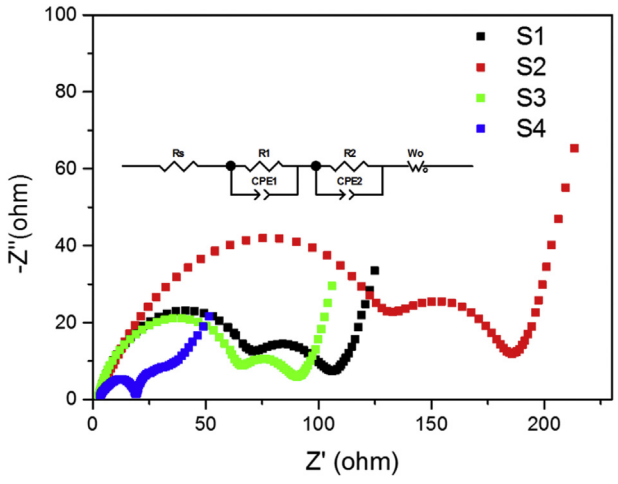

Fig. 5. Nyquist plots of the four sample electrodes after five cycle.

Acknowledgements

The authors gratefully acknowledge the financial support from the National High Technology Research and Development Program of China (Grant 2012AA110204), National Natural Science Foundation of China (Grant 21321062), National Found for Fostering Talents of Basic Science (Grant J1310024) and Key Project of Science and Technology of Xiamen (Grant2013H6022). The authors also appreciate the positive suggestions of Dr. Dong sun.

Appendix A. Supplementary data

Supplementary data related to this article can be found at http://dx.doi.org/10.1016/j.jpowsour.2016.03.051.

References

[1] J.M. Tarascon, M. Armand, Issues and challenges facing rechargeable lithium batteries, Nature 414 (2001) 359–367.
[2] K. Brandt, Historical development of secondary lithium batteries, Solid State Ionics 69 (1994) 173–183.
[3] B. Dunn, H. Kamath, J.M. Tarascon, Electrical energy storage for the grid: a battery of choices, Science 334 (2011) 928–935.
[4] P.G. Bruce, B. Scrosati, J.M. Tarascon, Nanomaterials for rechargeable lithium batteries, Angew. Chem.-Int. Ed. 47 (2008) 2930–2946.
[5] U. Kasavajjula, C. Wang, A.J. Appleby, Nano- and bulk-silicon-based insertion anodes for lithium-ion secondary cells, J. Power Sources 163 (2007) 1003–1039.
[6] X.H. Liu, L.Q. Zhang, L. Zhong, Y. Liu, H. Zheng, J.W. Wang, J.H. Cho, S.A. Dayeh, S.T. Picraux, J.P. Sullivan, S.X. Mao, Z.Z. Ye, J.Y. Huang, Ultrafast electrochemical lithiation of individual Si nanowire anodes, Nano Lett. 11 (2011) 2251–2258.
[7] M.N. Obrovac, L. Christensen, Structural changes in silicon anodes during lithium insertion/extraction, Electrochem Solid St. 7 (2004) A93–A96.
[8] M.N. Obrovac, L.J. Krause, Reversible cycling of crystalline silicon powder, J. Electrochem. Soc. 154 (2007) A103–A108.
[9] X.H. Liu, H. Zheng, L. Zhong, S. Huang, K. Karki, L.Q. Zhang, Y. Liu, A. Kushima, W.T. Liang, J.W. Wang, J.H. Cho, E. Epstein, S.A. Dayeh, S.T. Picraux, T. Zhu, J. Li, J.P. Sullivan, J. Cumings, C. Wang, S.X. Mao, Z.Z. Ye, S. Zhang, J.Y. Huang, Anisotropic swelling and fracture of silicon nanowires during lithiation, Nano Lett. 11 (2011) 3312–3318.
[10] B. Hertzberg, A. Alexeev, G. Yushin, Deformations in Si-Li anodes upon electrochemical alloying in nano-confined space, J. Am. Chem. Soc. 132 (2010) 8548–8549.
[11] L. Shi, W.K. Wang, A.B. Wang, K.G. Yuan, Y.S. Yang, Facile synthesis of scalable pore-containing silicon/nitrogen-rich carbon composites from waste contact mass of organosilane industry as anode materials for lithium-ion batteries, J. Mater Chem. A 2 (2014) 20213–20220.
[12] L.Y. Beaulieu, K.W. Eberman, R.L. Turner, L.J. Krause, J.R. Dahn, Colossal reversible volume changes in lithium alloys, Electrochem Solid St. 4 (2001) A137–A140.
[13] L.Y. Beaulieu, T.D. Hatchard, A. Bonakdarpour, M.D. Fleischauer, J.R. Dahn, Reaction of Li with alloy thin films studied by in situ AFM, J. Electrochem. Soc. 150 (2003) A1457–A1464.
[14] J. Graetz, C.C. Ahn, R. Yazami, B. Fultz, Highly reversible lithium storage in nanostructured silicon, Electrochem Solid St. 6 (2003) A194–A197.
[15] X.H. Liu, L. Zhong, S. Huang, S.X. Mao, T. Zhu, J.Y. Huang, Size-dependent fracture of silicon nanoparticles during lithiation, ACS Nano 6 (2012) 1522–1531.
[16] I. Ryu, J.W. Choi, Y. Cui, W.D. Nix, Size-dependent fracture of Si nanowire battery anodes, J. Mech. Phys. Solids 59 (2011) 1717–1730.
[17] H. Kim, M. Seo, M.H. Park, J. Cho, A critical size of silicon nano-anodes for lithium rechargeable batteries, Angew. Chem.-Int. Ed. 49 (2010) 2146–2149.
[18] Y. Yao, M.T. McDowell, I. Ryu, H. Wu, N.A. Liu, L.B. Hu, W.D. Nix, Y. Cui, Interconnected silicon hollow nanospheres for lithium-ion battery anodes with long cycle life, Nano Lett. 11 (2011) 2949–2954.
[19] C.K. Chan, H. Peng, G. Liu, K. Mcllwrath, X.F. Zhang, R.A. Huggins, Y. Cui, High-performance lithium battery anodes using silicon nanowires, Nat. Nanotechnol. 3 (2008) 31–35.
[20] H. Ma, F.Y. Cheng, J. Chen, J.Z. Zhao, C.S. Li, Z.L. Tao, J. Liang, Nest-like silicon

nanospheres for high-capacity lithium storage, Adv. Mater. 19 (2007) 4067–4070.
[21] Y.S. Hu, R. Demir-Cakan, M.M. Titirici, J.O. Muller, R. Schlogl, M. Antonietti, J. Maier, Superior storage performance of a Si@SiOx/C nanocomposite as anode material for lithium-ion batteries, Angew. Chem.-Int. Ed. 47 (2008) 1645–1649.
[22] Y.H. Xu, Y.J. Zhu, C.S. Wang, Mesoporous carbon/silicon composite anodes with enhanced performance for lithium-ion batteries, J. Mater Chem. A 2 (2014) 9751–9757.
[23] L. Yue, W.H. Zhang, J.F. Yang, L.Z. Zhang, Designing Si/porous-C composite with buffering voids as high capacity anode for lithium-ion batteries, Electrochim. Acta 125 (2014) 206–217.
[24] J. Shu, H. Li, R.Z. Yang, Y. Shi, X.J. Huang, Cage-like carbon nanotubes/Si composite as anode material for lithium ion batteries, Electrochem. Commun. 8 (2006) 51–54.
[25] Y.S. He, P.F. Gao, J. Chen, X.W. Yang, X.Z. Liao, J. Yang, Z.F. Ma, A novel bath lily-like graphene sheet-wrapped nano-Si composite as a high performance anode material for Li-ion batteries, RSC Adv. 1 (2011) 958–960.
[26] Z.P. Guo, D.Z. Jia, L. Yuan, H.K. Liu, Optimizing synthesis of silicon/disordered carbon composites for use as anode materials in lithium-ion batteries, J. Power Sources 159 (2006) 332–335.
[27] H. Kim, B. Han, J. Choo, J. Cho, Three-Dimensional porous silicon particles for use in high-performance lithium secondary batteries, Angew. Chem.-Int. Ed. 47 (2008) 10151–10154.
[28] N. Liu, Z. Lu, J. Zhao, M.T. McDowell, H.W. Lee, W. Zhao, Y. Cui, A pomegranate-inspired nanoscale design for large-volume-change lithium battery anodes, Nat. Nanotechnol. 9 (2014) 187–192.
[29] S.H. Ng, J. Wang, D. Wexler, K. Konstantinov, Z.P. Guo, H.K. Liu, Highly reversible lithium storage in spheroidal carbon-coated silicon nanocomposites as anodes for lithium-ion batteries, Angew. Chem. Int. Ed. Engl. 45 (2006) 6896–6899.
[30] H. Wu, G.Y. Zheng, N.A. Liu, T.J. Carney, Y. Yang, Y. Cui, Engineering empty space between Si nanoparticles for lithium-ion battery anodes, Nano Lett. 12 (2012) 904–909.
[31] D. Shao, D.P. Tang, J.W. Yang, Y.W. Li, L.Z. Zhang, Nano-structured composite of Si/(S-doped-carbon nanowire network) as anode material for lithium-ion batteries, J. Power Sources 297 (2015) 344–350.
[32] Y.S. Huang, D.Q. Wu, J.Z. Jiang, Y.Y. Mai, F. Zhang, H. Pan, X.L. Feng, Highly oriented macroporous graphene hybrid monoliths for lithium ion battery electrodes with ultrahigh capacity and rate capability, Nano Energy 12 (2015) 287–295.
[33] S. Li, X.Y. Qin, H.R. Zhang, J.X. Wu, Y.B. He, B.H. Li, F.Y. Kang, Silicon/carbon composite microspheres with hierarchical core-shell structure as anode for lithium ion batteries, Electrochem. Commun. 49 (2014) 98–102.
[34] D. Nan, Z.H. Huang, R.T. Lv, Y.X. Lin, L. Yang, X.L. Yu, L. Ye, W.C. Shen, H.Y. Sun, F.Y. Kang, Silicon-encapsulated hollow carbon nanofiber networks as binder-free anodes for lithium ion battery, J. Nanomater (2014) 1–10.
[35] J. Berger, M. Reist, J.M. Mayer, O. Felt, R. Gurny, Structure and interactions in chitosan hydrogels formed by complexation or aggregation for biomedical applications, Eur. J. Pharm. Biopharm. 57 (2004) 35–52.
[36] V.I. Lozinsky, I.Y. Galaev, F.M. Plieva, I.N. Savinal, H. Jungvid, B. Mattiasson, Polymeric cryogels as promising materials of biotechnological interest, Trends Biotechnol. 21 (2003) 445–451.
[37] L.G. Xue, G.J. Xu, Y. Li, S.L. Li, K. Fu, Q. Shi, X.W. Zhang, Carbon-coated Si nanoparticles dispersed in carbon nanotube networks as anode material for lithium-ion batteries, ACS Appl. Mater. Interfaces 5 (2013) 21–25.
[38] R. Mogi, M. Inaba, S.K. Jeong, Y. Iriyama, T. Abe, Z. Ogumi, Effects of some organic additives on lithium deposition in propylene carbonate, J. Electrochem. Soc. 149 (2002) A1578–A1583.
[39] T. Jiang, S.C. Zhang, X.P. Qiu, W.T. Zhu, L.Q. Chen, Preparation and characterization of silicon-based three-dimensional cellular anode for lithium ion battery, Electrochem. Commun. 9 (2007) 930–934.
[40] X.S. Zhou, Y.X. Yin, L.J. Wan, Y.G. Guo, Facile synthesis of silicon nanoparticles inserted into graphene sheets as improved anode materials for lithium-ion batteries, Chem. Commun. 48 (2012) 2198–2200.
[41] E. Luais, J. Sakai, S. Desplobain, G. Gautier, F. Tran-Van, F. Ghamouss, Thin and flexible silicon anode based on integrated macroporous silicon film onto electrodeposited copper current collector, J. Power Sources 242 (2013) 166–170.
[42] M.Y. Ge, J.P. Rong, X. Fang, C.W. Zhou, Porous doped silicon nanowires for lithium ion battery anode with long cycle life, Nano Lett. 12 (2012) 2318–2323.
[43] F.M. Hassan, V. Chabot, A.R. Elsayed, X.C. Xiao, Z.W. Chen, Engineered Si electrode nanoarchitecture: a scalable postfabrication treatment for the production of next-generation Li-ion batteries, Nano Lett. 14 (2014) 277–283.
[44] W. Sun, R.Z. Hu, H. Liu, M.Q. Zeng, L.C. Yang, H.H. Wang, M. Zhu, Embedding nano-silicon in graphene nanosheets by plasma assisted milling for high capacity anode materials in lithium ion batteries, J. Power Sources 268 (2014) 610–618.